Determining the Effect of Microstructure and Heat Treatment on the Mechanical Strengthening Behavior of an Aluminum Alloy Containing Lithium Precipitation Hardened with the δ' Al_3Li Intermetallic Phase

James M. Fragomeni and Ben M. Hillberry

(Submitted 2 December 1999)

The effect of the thermal treatment and composition on microstructure and subsequent mechanical behavior of an Al-2.6 wt.% Li-0.09 wt.% Zr alloy that was solution heat treated (SHT) and artificially aged for a series of aging times and temperatures was studied. The underaged, peakaged, and overaged thermal heat treatments were studied to determine the effect of the microstructure and processing on the mechanical properties. The precipitates in the microstructure, which impede dislocation motion and control the precipitation strengthening response as a function of aging practice, were analyzed as the basis for controlling the strengthening depending on their size distribution, average size, and interparticle spacing. The average particle size, spacing, and size distribution were determined from the microstructure as a function of the thermal processing and composition. For the demonstration alloy, the primary strengthening was a direct consequence of ordered coherent Al_3Li (δ') intermetallic precipitates, which are uniformly distributed throughout the microstructure and restrict the glide motion of dislocations during plastic deformation. The Al_3Li average particle size, distribution, spacing, and volume fraction are closely related to the overall mechanical behavior and are a result of the heat treating practice and composition. Consequently, a micromechanical model was developed for predicting the precipitation hardening response in terms of the variation in polycrystalline strength with aging time, aging temperature, and composition. The overall micromechanical model, which was determined from the particle coarsening kinetics, dislocation mechanics, thermodynamics, resolved shear stress, as well as the dislocation particle shearing and bypassing mechanisms, accurately predicted the mechanical strength in the underaged, peak-aged, and overaged tempers of the demonstration alloy.

Keywords aluminum, microstructure, precipitation hardening

1. Introduction

The aging response of a metal or alloy can be determined from the microstructure *via* the composition and the heat treatment. The composition and the heat treatment determine the particle size distribution (PSD), which can be used as the basis to predict the precipitation hardening response. The heat treatment variables include the aging practice (temperature and time), and the solution heat treatment practice. The precipitation hardening response includes the underaged, peak-aged, and overaged conditions. The heat treatment influences the microstructural particle-strengthening mechanisms through the precipitate size, volume fraction, and precipitate size distribution. The particles of the distribution, distributed randomly throughout the microstructure, interact with and impede the dislocation motion to strengthen the alloy. For alloys strengthened by coherent deformable particles, the dislocations often shear the precipitates in the underaged condition and usually loop the precipitates in the overaged condition. In the peak-aged condition, a combination of particle shearing and particle looping can sometimes occur simultaneously to determine the precipitation strengthening response of the alloy due to a distribution of both large and small particle sizes. The CRSS results from the interaction of the dislocations with the randomly distributed precipitates and is the amount of stress necessary for the dislocations to bypass and/or shear the precipitates in a single crystal of material. Most of the models used to predict the overall strength of a metal or alloy are based on the CRSS. From the CRSS, the polycrystalline yield strength can be estimated by using the Taylor factor.

The precipitation strengthening response of an alloy can be determined from the active microstructural particle-strengthening mechanisms, which contribute to the CRSS of the alloy in the underaged, peakaged, and overaged conditions. Different particle-strengthening mechanisms can occur at different aging times depending on the alloy and the size, distribution, morphology, and spacing of the precipitates in the microstructure. Some of the different particle-strengthening mechanisms include, for example, coherency strengthening,[1,2] stacking fault strengthening,[3] modulus strengthening,[4,7] chemical strengthening,[8] order hardening,[9,13] and Orowan strengthening.[14] For a given precipitation strengthened alloy, one or more of these particle-strengthening mechanisms can be active and make a non-negligible contribution to the overall strength.

James M. Fragomeni, Department of Mechanical Engineering, Ohio University College of Engineering & Technology, Athens, OH 45701; and **Ben M. Hillberry**, School of Mechanical Engineering, Purdue University, West Lafayette, IN 47907.

The material used as the demonstration alloy for this research was a precipitation-hardened aluminum-lithium (Al-Li) alloy. This alloy was selected as the vehicle to relate the strength to the microstructure, heat treatment practice, and composition. The variation in strength with aging time, temperature, and composition can be predicted utilizing a number of existing models that describe dislocation mechanics, particle coarsening, thermodynamics, and particle-strengthening mechanisms applicable to precipitation-hardened alloys. For the demonstration alloy, the primary strengthening contribution comes from δ' (Al_3Li) particles randomly distributed throughout the microstructure, which impede dislocation motion. The misfit of these precipitates is extremely small ($\sim -0.1\%$), so the strengthening contribution is almost entirely due to the ordered structure of the precipitate and is a function of the sheared cross-sectional diameter only.[15] The δ particle size, and distribution are closely related to the precipitation strengthening response and are a direct consequence of the aging practice and composition.

The Al-Li alloys offer some attractive benefits over conventional aluminum alloys for aerospace structural applications. For aerospace applications, Al-Li alloys provide a direct weight-saving benefit and an improved elastic modulus over conventional 2XXX and 7XXX aluminum alloys. The addition of lithium to aluminum results in a 3% decrease in density and a 6% increase in elastic modulus for each weight percent of lithium added to the alloy. The decreased density and improved elastic modulus of Al-Li alloys provide a cost-effective advantage over the conventional 2XXX and 7XXX alloys used in aircraft structures. For example, alloys 2090, 8090, and 2091 have been used in a variety of commercial aircraft, military aircraft, and aerospace applications. In addition, the Aluminum Company of America (ALCOA, Alcoa Research Center, Pittsburgh, PA) announced the first Al-Li alloy, X2020, in 1958 as a plate product for use on the RA-5C Vigilante military aircraft, and since then, numerous other Al-Li alloys have been developed in plate, sheet, billet, and extruded forms.

From a detailed study of the strengthening mechanism applicable to the Al-Li alloy system, it was found that order hardening controlled the strengthening when the δ' precipitates were sheared by the dislocations and Orowan hardening controlled the strengthening in the overaged condition when the dislocations looped the particles. Using the appropriate models for these strengthening mechanisms, analytical predictions were made for the single crystal strength. The single crystal strength was then used as the basis to predict the polycrystalline strength.

2. Experimental Methods

2.1 Material Processing

An aluminum-lithium-zirconium alloy having a composition of 2.6 wt.% Li and 0.09 wt.% Zr (Table 1) was cast by ALCOA at and was used as the demonstration alloy for this investigation. The complete composition analysis was performed by ALCOA using optical emission spectrometric analysis. One large ingot (2250 kg) was cast by the ALCOA Laboratories due to the difficulty in reproducibility of casting several small ingots. The casting was rolled into a slab having dimensions of 30.5 cm (12 in.) × 96 cm (38 in.) × 30.5 cm (12 in.).

Table 1 Composition analysis determined by optical emission spectrometric analysis for the Al-Li-Zr research alloy

Al	Li	Zr	Cu	Mg	Si	Fe	Ti	B	Na	Ca
Bal	2.59	0.09	0.11	0.07	0.04	0.03	0.01	<0.001	<0.001	<0.001

The ingot was later preheated in a gas-fired furnace for a total time of 20 h. The first 8 h was in a furnace temperature range of 482 to −500 °C and the last 12 h in a furnace temperature range of 527 to −538 °C. Several billets were then machined from the preheated ingot, having the dimensions of 15.25 cm (6 in.) in diameter and 25.4 cm (10 in.) or 50.8 cm (20 in.) in length, to be used for the extrusion processing of the demonstration alloy.

2.2 Extrusion Processing

The aluminum-lithium-zirconium billets were direct extruded by ALCOA at their Lafayette Extrusion and Tube Division after being reheated to temperatures of approximately either 466 °C or 290 °C. Six product geometries were extruded from the billets using an instrumented 2500 t press in the direct mode.[2] The product geometry used for this investigation was a 1.91 cm (0.75 in.) diameter round extruded rod in the longitudinal grain direction. The extrusion ratio was 73:1 and the corresponding aspect ratio was 1:1 for the round rod geometry. An extrusion temperature of approximately 339 °C was used for the Al-Li-Zr demonstration alloy.

2.3 Extrusion Post-processing

The Al-Li alloy was machined into tensile samples from the extruded product. The tensile samples were oriented in the longitudinal grain direction. The tensile samples were first solution heat treated (SHT) for 1 h at 550 °C in a molten sodium nitrate salt solution followed by a cold water quench to room temperature. Following the solution heat treatment, the tensile samples were artificially aged for various lengths of time in a molten sodium nitrate ($NaNO_3$) salt bath. Different aging treatments were utilized by varying both the time and the temperature. The samples were immediately quenched in cold water, at approximately room temperature, after the artificial aging treatment. The samples were aged at temperatures of 185 and 193 °C. The molten salt solution was continuously stirred throughout the solution heat treatment and aging process to ensure a uniform temperature distribution throughout the bath.

2.4 Monotonic Tensile Tests

The experimentally determined values for the tensile properties along the longitudinal direction were obtained from mechanically testing the heat-treated tensile samples. Tensile testing was performed in accordance with the American Society for Testing and Materials (ASTM) B557M[16] test specifications. All the tensile testing was performed at room temperature with the test machine operating in stroke control. The mechanical testing was performed utilizing a ±22 kip (100 KN) MTS System Corporation electrohydraulic testing system in the

Purdue Mechanical Engineering Department's Materials Laboratory. For the purposes of this investigation, round rod tensile samples were machined from the round geometry extruded product in the longitudinal grain direction. The tensile samples were tested in the longitudinal orientation. It has been previously shown[17] that tensile data from the material extruded by ALCOA was reproducible, so therefore, one tensile test was performed for each aging time and temperature.

2.5 Transmission Electron Microscopy

The PSD and particle morphology were examined and photographed using transmission electron microscopy (TEM) from thin foil specimens obtained from samples aged at 185 °C for different aging times ranging from 24 h to 225 h. The thin foil specimen was sliced with a diamond blade saw cutter and then polished to foils approximately 0.05 mm thick. Disks approximately 3 mm in diameter were then punched from the thin foils. The thin foil disks were then electropolished using a twin jet polisher, with the disks submerged in a 3:1 methanol-nitric acid solution cooled by liquid nitrogen to around −20 to −35 °C. The thin foil disks were observed and photographed using a JEOL-200CX microscope (Japan Electron Optics Ltd., Tokyo) operating at 200 kV for various specimen inclinations. Particle size measurements of the δ' (Al_3Li) precipitates were made directly from TEM negatives. A semiautomatic EyeCom II image analyzing system was used to measure particle sizes.

3. Theoretical Approach

3.1 Predicting the Precipitation Strengthening Response

The aging response for the Al-Li alloy was predicted by determining the contributions from the active microstructure strengthening mechanisms to the critical resolved shear strength, (CRSS), in the underaged, peak-aged, and overaged conditions. The CRSS was predicted from analytical models that describe the various active microstructure particle-strengthening mechanisms in Al-Li alloys. A variety of particles-strengthening mechanisms were evaluated to determine which mechanisms would be appropriate in describing the Al-Li aging behavior. The CRSS for each incremental particle-strengthening mechanism was predicted by using the PSDs that were determined from the microstructure model. The models for the particle-strengthening mechanisms that were found to make significant contributions to the CRSS were incorporated into a computer-based model for materials design. The particle-strengthening mechanisms evaluated include coherency strengthening, chemical strengthening, modulus strengthening, stacking fault strengthening, order strengthening, and Orowan strengthening. Predictions were made for all of the strengthening mechanisms at each given aging time utilizing the appropriate analytical models, which describe these strengthening mechanisms. In addition, an extensive review of the literature was performed for these strengthening mechanisms in reference to the strengthening behavior of the Al-Li alloy system to determine which mechanisms were most applicable in describing the strengthening behavior of the Al-Li alloy.

From the review of the literature, it was found that order strengthening was the most predominate particle-strengthening mechanism for the Al-Li alloy system when the δ' particles are sheared by the dislocations. Huang[18] and Huang and Ardell[19, 20, 21] concluded that order hardening accounts for the particle-strengthening contribution from dislocation shearing the δ' precipitates. Sainfort and Guyot[22] also found for Al-Li alloys containing 2, 2.5, and 3.0 wt.% Li that order and Orowan strengthening mechanisms were responsible for the strength contribution from the δ' precipitates. Glazer,[13] Glazer and Morris,[15] and Glazer *et al.*[23] also indicated that order hardening is the primary mechanism that controls the strengthening response for δ' shearing in Al-Li alloys and used it as the basis to predict the age-hardening curve for an Al-Li-Mn alloy up to peak strength. Noble *et al.*[24] found that the strengthening from δ' particles is primarily due to order strengthening or possibly a combination of order and modulus hardening for four different polycrystalline Al-Li alloy compositions. Huang has clearly shown that the contributions due to coherency, chemical, modulus, and stacking fault strengthening to the total strength are all negligibly small for the Al-Li alloy system. In addition, Huang[18] found that strengthening due to δ' particles in overaged alloys was by the Orowan bypassing mechanism. In summary, Huang concluded that the contribution of other hardening mechanisms involved in the strengthening due to δ' precipitates is unimportant.[18] Gomiero et al.[25] found that for Al-Li, the contribution for precipitation hardening can be attributed to antiphase boundary formation, *i.e.*, order hardening, and contributions from other strengthening mechanisms are negligible for the δ' precipitates. These findings were consistent with those of this investigation.

From calculations performed in this research using the analytical models that describe the strengthening, the particle-hardening mechanisms that were found to contribute to the strengthening were primarily from order strengthening and Orowan strengthening. Using the appropriate values for the microstructural constants determined from the literature for the Al-Li alloy, it was found that the contributions from chemical strengthening, coherency strengthening, modulus strengthening, and stacking fault strengthening all contributed less than 5 to 7% to the total strength. As a consequence, these strengthening mechanisms were found to make negligible contributions to the CRSS for the Al-Li alloy studied in this research. However, even though these strengthening mechanisms were not found to be descriptive of the dislocation particle strengthening for the Al-Li research alloy, they were considered as applicable to some other particle-hardened alloys.

The aging curve was predicted for the Al-Li alloy for aging times up to 225 h. A PSD was determined by a microstructural model for each aging time and was used to help predict the single crystal strength. The predictions for the CRSS were determined from either or both of the predominant strengthening mechanisms depending on the PSD for the given aging time. The analytical models corresponding to these particle-strengthening mechanisms were based on the statistical interaction of dislocations with a random array of particles. This was applicable to the Al-Li alloy system since Al-Li alloys have a relatively random distribution of precipitates throughout the microstructure. A description of the analytical models that were incorporated into the overall model is given in the next sections of this paper.

3.2 Precipitation Strengthening Model

Order Strengthening. In this section, a model is presented that describes the observed increase in the CRSS due to ordered coherent precipitates. The theory is based on the assumption that there exists a statistical distribution of particle sizes present in the matrix phase of the alloy. When dislocations shear particles with an ordered structure, this results in the creation of an antiphase boundary on the slip plane of the particle. The antiphase boundary energy represents the force opposing the glide of a dislocation as it shears the ordered precipitates. Modeling of order strengthening is detailed and depends in part on the size and spacing of precipitates, as described by Brown and Ham.[9] Ardell[12] revised Brown and Ham's theory of order strengthening to include the contribution of both dislocations of the pair on the CRSS. In the underaged condition, when the precipitates are small in size, the theoretical CRSS due to order hardening, $\Delta\tau_{\text{order}}$, is given by[12,18]

$$\Delta\tau_{\text{order}} = \frac{\gamma_{\text{apb}}}{2\mathbf{b}}\left[\left(\frac{3\pi^2\gamma_{\text{apb}} f_{\delta'}\bar{r}}{32\Gamma}\right)^{1/2} - f_{\delta'}\right] \quad \text{(Eq 1)}$$

or

$$\Delta\tau_{\text{order}} = \frac{\gamma_{\text{apb}}}{2\mathbf{b}}\left(\frac{3\pi^2\gamma_{\text{apb}} f_{\delta'}\bar{r}}{32\Gamma}\right)^{1/2} \quad \text{(Eq 2)}$$

where γ_{apb} is the antiphase boundary energy, **b** is the Burgers vector of the dislocation, Γ is the line tension of the dislocation, $\bar{r}$ is the average particle size radius, and $f_{\delta'}$ is the volume fraction of the δ' precipitates. A detailed discussion is given in Sections 4.1–4.4 on determining the dislocation line tension, precipitate volume fraction, and antiphase boundary energy in reference to the Al-Li alloy system. Equation 1 applies when the trailing dislocation of the pair remains straight. However, when the trailing dislocation of the pair bends through the sheared δ' precipitates, Eq 2 applies. It has been determined[12,18,20,21] that Eq 2 is applicable for predicting the strengthening by ordered coherent δ' particles in Al-Li alloys. In the peak-aged condition, the δ' precipitates are larger than in the underaged condition and therefore have increased resistance to dislocation glide. The theoretical CRSS can be approximated in the peak-aged condition for order hardening by the expression given by[9,12,18]

$$\Delta\tau_{\text{order}} = 0.81\,\frac{\gamma_{\text{apb}}}{2\mathbf{b}}\left[\left(\frac{3\pi f_{\delta'}}{8}\right)^{1/2} - f_{\delta'}\right] \quad \text{(Eq 3)}$$

or

$$\Delta\tau_{\text{order}} = 0.81\,\frac{\gamma_{\text{apb}}}{2\mathbf{b}}\left(\frac{3\pi f_{\delta'}}{8}\right)^{1/2} = \frac{\gamma_{\text{apb}}\sqrt{f_{\delta'}}}{2.275\mathbf{b}} \quad \text{(Eq 4)}$$

As with the underaged condition, Eq 3 applies when the trailing dislocation of the pair remains straight, and Eq 4 is appropriate when the dislocation is pulled through the sheared precipitates. Equation 4 is applicable for δ' strengthening of peak-aged Al-Li alloys.[12,18,20,21] For the demonstration Al-Li alloy, Eq 2 and 4 were utilized in making predictions for the strength.

Orowan Strengthening. Once the precipitates have grown larger than a critical particle size, the dislocations bypass the precipitates. The mechanism by which dislocations bypass precipitates was first proposed by Orowan[14] and is referred to as the Orowan mechanism. For overaged Al-Li, Furukawa *et al.*[26,27] concluded that the dislocations by-pass the δ' particles leaving dislocation loops around them by the Orowan mechanism. The Orowan model can be expressed in its simplest form as[14]

$$\Delta\tau_{\text{orowan}} = \frac{G_t\mathbf{b}}{\lambda} \quad \text{(Eq 5)}$$

where G_t is the shear modulus of the material, **b** the Burgers vector, and λ the interparticle spacing. This expression is applicable for order-of-magnitude calculations of the strengthening increment for particles of known average spacing. A more refined version of the Orowan model is required for purposes of determining more accurate predictions of the strengthening. The basic Orowan model has been refined over the years to include a more accurate estimate of the interparticle spacing and the effect of the bowed-out dislocation segments on the dislocation line tension. These factors have been incorporated into Eq 5 to provide a more exact model for the Orowan strengthening.

Interparticle Spacing. The parameter λ can be approximated by the mean square lattice spacing. The mean square lattice spacing, L_s, is given by the expression

$$L_s = \bar{r}\sqrt{\frac{2\pi}{3f_{\delta'}}} \quad \text{(Eq 6)}$$

Thus, the Orowan expression becomes

$$\Delta\tau_{\text{orowan}} = \frac{2\Gamma}{\mathbf{b}\bar{r}}\left(\frac{3f_{\delta'}}{2\pi}\right)^{1/2} \quad \text{(Eq 7)}$$

However, the mean square lattice spacing is not always appropriate in determining the distance between particles. In determining the interaction between a gliding dislocation with a random array of obstacles in its slip plane, the average distance from a particle to its nearest two, three, or four neighbors (instead of its nearest neighbor) is the correct estimate.[28] Foreman and Makin[29] and Kocks[30] have considered this problem in their computer simulation experiments and have found that, in general, the more nearest neighbors that are considered, the greater will be the effective interparticle separation. They have shown that L should be greater than L_s such that

$$L_s^{-*} = \frac{1}{0.81}\,\bar{r}\left(\frac{2\pi}{3\phi_{\delta'}}\right)^{1/2} \quad \text{(Eq 8)}$$

where L_s^{-*} is the effective mean square lattice spacing. Hence, the contribution to the CRSS due to Orowan strengthening can be expressed as

$$\Delta\tau_{\text{orowan}} = 0.81\,\frac{2\Gamma}{\mathbf{b}\bar{r}}\left(\frac{3f_{\delta'}}{2\pi}\right)^{1/2} \qquad \text{(Eq 9)}$$

Equation 9 is the appropriate expression provided that the average particle size is much smaller than the interparticle separation. If this is not the case, then the surface-to-surface mean planar separation of particles, λ_s^*, must be used. This parameter can be expressed as

$$\lambda_s^* = \bar{L}_s^* - 2\bar{r}_s \qquad \text{(Eq 10)}$$

where $\bar{r}$ ($=\pi\bar{r}/4$) is the average planar radius. Therefore, substituting the expressions $\bar{r}$ and $\bar{L}_s^*$ into Eq 10 yields

$$\lambda_s^* = \bar{r}\left[\frac{1}{0.81}\sqrt{\frac{2\pi}{3f_{\delta'}}} - \frac{\pi}{2}\right] \qquad \text{(Eq 11)}$$

Thus, the Orowan stress can be expressed as

$$\Delta\tau_{\text{orowan}} = 0.81\,\frac{2\Gamma}{\mathbf{b}\bar{r}\left[\sqrt{\frac{2\pi}{3f_{\delta'}}} - \frac{\pi}{2}\right]} \qquad \text{(Eq 12)}$$

Dislocation Dipole Effect. Ashby[31] studied the influence of the interaction between the two arms of a bowing dislocation on either side of a particle. There is an attractive force between the dislocation arms since the arms have opposite signs. This will reduce the stress necessary for the dislocation to bypass the particles. The two segments of the bowing dislocation form a dislocation dipole with a separation equal to the particle diameter. Ashby modified the Orowan stress by writing the logarithmic term in the dislocation line tension equation as ln (Λ/r_{ic}). The term r_{ic} is the dislocation inner cut-off radius, often taken as equal in magnitude to twice the Burgers vector of the dislocation, and Λ is the outer cut-off radius for the dislocation line tension, taken as equal to $2\bar{r}_s$. Incorporating these parameters into the basic Orowan model yields a more exact theoretical estimate for the Orowan stress. The final expression is given by:

$$\Delta\tau_{\text{orowan}} = 0.81\,\frac{G_m\mathbf{b}}{2\pi\bar{r}\sqrt{(1-\nu)}}\left(\frac{3f_{\delta'}}{2\pi}\right)^{1/2}\ln\left(\frac{\bar{r}_s}{\mathbf{b}}\right) \qquad \text{(Eq 13)}$$

Equation 13 applies when the average particle size is much smaller than the interparticle spacing. When the particle diameter is not much smaller than the interparticle spacing, *i.e.*, when the particle spacing is not much greater than the particle diameter, the Orowan equation is given by

$$\Delta\tau_{\text{orowan}} = 0.81\left[\frac{G_m\mathbf{b}}{2\pi\bar{r}\sqrt{(1-\nu)}\left(\sqrt{\frac{2\pi}{3f_{\delta'}}} - \frac{\pi}{2}\right)}\right]\ln\left(\frac{\bar{r}_s}{\mathbf{b}}\right) \qquad \text{(Eq. 14)}$$

where G_m is the shear modulus of the matrix phase, ν is the Poisson's ratio, $\bar{r}_s$ is the average planar radius, and **b** is the Burgers vector. Equation 13 and 14 were utilized in making predictions for the demonstration alloy.

4. Evaluating the Model Parameters

4.1 Minimum Particle Radius for Orowan Looping

As the precipitates grow and coarsen, their spacing increases concurrently with their size. Eventually, they will reach a critical particle size where the dislocation looping of particles becomes easier than dislocation shearing of particles. The minimum radius for Orowan looping is achieved when the particle size reaches the point of equality in the force balance between the stress for precipitate shearing and Orowan looping. At the limit between these two processes, the strengthening for some alloy systems goes through a maximum. However, for some systems, the maximum in strength occurs prior to the particle shearing-looping transition. Before there is Orowan looping for all of the particles of the size distribution, there is a transition in which both Orowan looping and particle shearing simultaneously occur for a given distribution. The precipitates are never monodispersed because of the statistical distribution of particle sizes in which the large precipitates are bypassed and looped by the dislocations, and the small precipitates are sheared by dislocations.

Several investigators have experimentally measured the Orowan looping radius for the Al-Li alloy system. Sainfort and Guyot[32] determined a critical looping radius of 17.5 nm for an Al-3 wt.% Li alloy ($f_v = 0.25$) aged at 220 °C. Furukawa *et al.*[27] used a value of 25 nm for an Al-3 wt.% Li aged at 200 °C. The aging temperature should not change the value of the critical looping radius, since it is the critical size that determines the looping mechanism. These experimental values can be measured from the size of the smallest Orowan loops observed by TEM on plastically deformed alloys or deduced from the mean precipitate size of the δ'-PSD at maximum strength. An average value of the δ' PSD at peak strength can be determined from the microstructural model. Using this second approach, a minimum Orowan looping radius of 13.5 nm was determined for the Al-Li-Zr demonstration alloy based on the average δ' particle size in the peak-aged condition.

4.2 Antiphase Boundary Energy

Critical to the success of predicting the CRSS is an accurate determination of the antiphase boundary energy, γ_{apb}, on the {111} slip planes of the precipitate phase. The antiphase boundary will result on the {111} planes when the ordered δ' precipitates are sheared during deformation by the dislocation pairs. Several investigators attempted to determine the antiphase boundary energy by measuring the separation distance between dislocation pairs. Using this method, Tamura *et al.*[33] determined the antiphase boundary energy to equal 0.195 J/m^2 for an Al-2 wt.% Li alloy. For polycrystalline Al-2.5 wt.% Li alloys aged at 200 °C, Sainfort and Guyot[32] obtained values of 0.130 and 0.175 J/m^2 using this technique. From a detailed investigation analyzing the published data of several investigators on

the strengthening of Al-Li alloys by δ' precipitates, Ardell and Huang[34] determined that the antiphase boundary energy on {111} of the γ' phase lies between 0.140 and 0.160 J/m^2. They also concluded this to be in excellent agreement with the average value of 0.151 ± 0.008 J/m^2 obtained from the analysis of the δ' strengthening contribution in ternary Al-Li-Cu alloys.[20,34] Based on the above results for the antiphase energy of Al-Li alloys on {111} of δ' precipitates, for the demonstration alloy studied in this investigation, a value of 0.150 J/m^2 was utilized for γ_{apb} for calculating the contribution from order hardening to the CRSS. This value was used as representative of the range of experimental values that γ_{apb} varies. However, as Glazer[13] points out, the effective antiphase boundary energy may change with precipitate radius, composition, and/or temperature.

4.3 Dislocation Line Tension

In order to best utilize the above expressions for the CRSS, a meaningful estimate of the dislocation line tension is required. This is necessary since in real materials the line tension of the dislocation is not constant but varies with the angle ξ between the dislocation line and the Burgers vector. The generalized formula for the dislocation line tension can be approximated according to the De Wit-Koehler model given by[35]

$$\Gamma = \frac{G_m \mathbf{b}^2}{4\pi}\left[\frac{1 + \nu + 3\nu\sin^2\xi}{1 - \nu}\right]\ln\left(\frac{A}{r_{ic}}\right) \quad \text{(Eq 15)}$$

where G_m is the shear modulus of the matrix on {111} and ξ is the angle between **b** and the dislocation line. The terms A and r_{ic} are, respectively, the outer and inner cut-off distances for calculating the line energy. $\xi = 0$ for a pure screw dislocation and $\xi = \pi/2$ for a pure edge dislocation. The value of A can be approximated by the Friedel spacing, $L_F = 2\bar{r}_s$, where $\bar{r}_s$ is the average planar radius of the precipitates and $r_{ic} = 2\mathbf{b}$. The value of r_{ic} can also be taken as equal to **b**[34]. However, when the particles have grown larger around the peak-aged condition, Γ can be approximated as[36]

$$\Gamma = \frac{G_m \mathbf{b}^2}{4\pi(1 - \nu)^{1/2}}\ln\left(\frac{A}{r_{ic}}\right) \quad \text{(Eq 16)}$$

where A is given by $((2\bar{r}_s)^{-1} + L_s^{-1})^{-1}$. When the volume fraction of δ' is small, less than 0.1, A can be approximated by $2\bar{r}_s$. Since the dislocation character has been found to be primarily screw type,[26,27,37] in binary Al-Li single crystals and using a value of $\nu = 0.339$,[38,39] the De Wit Koehler model can be expressed as

$$\Gamma = 2.026\,\frac{G_m \mathbf{b}^2}{4\pi}\ln\left(\frac{L_F}{2\mathbf{b}}\right) \quad \text{(Eq 17)}$$

where

$$L_F = 2\bar{r}_s = \frac{\pi\bar{r}}{2} \quad \text{(Eq 18)}$$

Table 2 Values for some of the microstructural variables used for determining the CRSS of the Al-2.6 wt. % Li-0.09 wt. % Zr research alloy aged at 185 °C

Aging time (h)	Average particle radius (A)	Dislocation line tension G (nN)	Number of particles looped (r_{loop} = 135 A)
0.12	18.8	0.78707	0
0.25	24.0	0.88478	0
0.50	30.2	0.97706	0
1.0	38.1	1.0693	0
2.0	48.0	1.11616	0
4.0	60.5	1.2539	0
8.0	76.2	1.3462	3
12.0	87.2	1.4001	5
18.0	99.9	1.4541	14
24.0	109.9	1.4924	27
32.0	121.0	1.5307	48
40.0	130.3	1.5604	76
48.0	138.5	1.5847	108
72.0	158.5	1.6387	139
96.0	174.5	1.6770	165
120.0	188.0	1.7067	165
180.0	215.2	1.7607	184
225.0	231.8	1.7904	197

Table 3 Values for some of the microstructural variables used for determining of the Al-2.6 wt.% Li-0.09 wt.% Zr research alloy aged at 193 °C

Aging time (h)	Average particle radius (A)	Dislocation line tension G (nN)	Number of particles looped (r_{loop} = 135 A)
0.12	21.5	0.84149	0
0.25	27.5	0.93920	0
0.50	34.7	1.0315	0
1.0	43.7	1.1238	0
2.0	55.0	1.2160	0
4.0	69.3	1.3083	0
8.0	87.3	1.4006	5
12.0	100.0	1.4546	14
18.0	114.4	1.5085	48
24.0	126.0	1.5468	76
32.0	138.6	1.5851	108
40.0	149.3	1.6148	108
48.0	158.7	1.6275	139
72.0	181.7	1.6688	165
96.0	200.0	1.7071	165
120.0	215.4	1.7611	184
180.0	246.6	1.8151	197
225.0	265.6	1.8448	197

For all of the numerical calculations, **b** = 0.2864 nm[32] and G_m = 30.2 GPa.[38] Tables 2 and 3 provide the calculated values for Γ for aging temperatures of 185 and 193 °C, respectively, utilizing the De Wit-Koehler model applicable to Al-Li dislocation behavior.

4.4 Volume Fraction

The volume fraction of precipitate is an important parameter influencing the precipitation strengthening response of particle-hardened alloys. The exact value of the volume fraction for a given microstructural precipitate can be difficult to determine. In a few alloy systems, the volume fraction of the precipitate particles is constant from the onset of aging, whereas with many alloys, the volume fraction will increase with aging until the equilibrium value is achieved. For the Al-Li demonstration alloy utilized in this research, the volume fraction can be assumed to be essentially constant.[40] For Al-Li alloys, the volume fraction is essentially constant during coarsening for reasonable initial volume fraction and precipitate sizes.[13] A constant value for the volume fraction of δ' has been assumed for some other Al-Li alloys.[41–51] However, in contrast to the work of Mahalingam *et al.*,[50, 51] several investigators[26,27,33,37] have claimed that the volume fraction of δ' increases with aging time in the underaged condition until the equilibrium volume fraction is reached. The equilibrium or final volume fraction of precipitate can be estimated from the δ' solvus line of the equilibrium Al-Li phase diagram. For the Al-2.6 wt.% Li alloy studied in this research, the equilibrium volume fraction is approximately 0.16. The equilibrium value for the volume fraction was used for this investigation based on the work of Gu, Mahalingam, and Sanders.[41–51] This value compares with that of Sainfort and Guyot,[22,52] who used a constant value of 0.15 for the δ' volume fraction throughout the aging response of some polycrystalline Al-2.5 wt.% Li alloys. For polycrystalline Al-3 wt.% Li, Sainfort and Guyot[22] used a value of 0.25 for the δ' volume fraction throughout the aging response, and for Al-2 wt.% Li, a constant value of 0.05 was used for their volume fraction.

However, it should be noted that as the aging process continues in a severely overaged condition, the δ' precipitates will coarsen in the severely overaged state and the heterogeneous precipitation and growth of a δ (AlLi) phase may likely occur at the grain boundaries. The preferential growth of the δ phase at the grain boundaries results in the dissolution of the δ' particles in the vicinity of the grain boundaries.[48] This can lead to a decrease in the volume fraction of the δ' precipitates as well as the formation of a precipitate free zone (PFZ). Jha *et al.*[48] describes the PFZ formation in Al-Li alloys by the growth of equilibrium δ particles at the grain boundaries.

4.5 Predicting the Particle Size, Growth Rate, and Size Distribution

To develop a model for predicting the precipitation-hardening response, the PSD and the average particle size, for each selected aging time along the age-hardening curve, must be predicted. For Al-Li alloys, the precipitates coarsen according to the Lifshitz-Slyozov-Wagner (LSW) coarsening theory even at very small sizes.[53,54] The average particle size can therefore be determined from the LSW[55,56] cubic coarsening theory, which can be expressed by the relation

$$\bar{r}^3 - r_o^3 = K_c t \qquad \text{(Eq 19)}$$

where r_o is the initial particle size (at $t = 0$) and can be taken as approximately equal to zero for the Al-Li demonstration alloy. The growth rate constant K_c, at small volume fractions K_{co}, is given by the expression[55,56]

$$K_{co} = \frac{8\gamma V_m^2 C_{eq} D}{9\mathrm{R}T} \qquad \text{(Eq 20)}$$

where T is the aging temperature, R is the universal gas constant, K_{co} is the rate constant, D is the diffusion coefficient, γ is the interfacial energy, C_{eq} is the equilibrium concentration of the solute in the matrix, and V_m is the molar volume of the precipitate. It is known that this expression for K_{co} is valid for very small volume fractions, while supposedly more realistic rate constants are dependent on $f_{\delta'}$.[18, 57] There have been modifications[57,58,59] to the LSW model given in Eq 20 to take into account the volume fraction dependence of the coarsening rate. For example, Ardell[57] modified the LSW theory to account for the high volume fraction effect on K_{co} in some alloys. The modified version of the LSW theory is referred to as the modified LSW theory and can be expressed in terms of the rate constant as[57]

$$K_{fv} = \frac{6\gamma V_m^2 C_{eq} D}{\mathrm{R}T} \frac{\bar{\rho}_{fv}^3}{\nu_{fv}} \qquad \text{(Eq 21a)}$$

and

$$\frac{\bar{\rho}_{fv}^3}{\nu_{fv}} = \frac{4K_{fv}}{27K_{co}} \qquad \text{(Eq 21b)}$$

where K_{fv} is the growth rate constant at a given volume fraction of f_v, K_{co} is the growth rate at very small volume fractions, $\bar{\rho} = \bar{r}/r_c$ is the relative radius, ν_{fv} is a function related to volume fraction and constant time dt/dr_c^3, and r_c is the critical particle radius of the polydisperse system.[57] When $f_v = 0$, then $\nu_{fv} = 27/4$, and Eequation (21) reduces to the LSW theory, Eq 20.[46,57] The growth rate can also be expressed in terms of the activation energy for diffusion given by the relation[60]

$$K_c = \frac{C_k}{T} \exp\left[\frac{-Q_A}{\mathrm{R}T}\right] \qquad \text{(Eq 22)}$$

where Q_A is the activation energy, T is the aging temperature, C_k is the kinetic constant, and R is the universal gas constant. The cubic coarsening expression can therefore be expressed by the relation[55,56,60]

$$\bar{r}^3 - \bar{r}_o^3 = \frac{C_k t}{T} \exp\left[\frac{-Q_A}{\mathrm{R}T}\right] \qquad \text{(Eq 23)}$$

Alternatively, the growth rate can be written in terms of the composition and aging practice for the Al-Li demonstration alloy. Based on the microstructural model[41–51] along with some data generated by some other investigators investigators,[61,62] a simple empirical expression relating lithium content, aging temperature, and aging time may be determined as[50]

$$\ln\{K_c T\} = \frac{b}{T} + c \quad \text{(Eq 24)}$$

where b and c can be expressed as functions of lithium content given by[50]

$$b = -2545.73(\text{wt.\% Li}) - 4749.06 \quad \text{(Eq 25a)}$$

$$c = 5.88(\text{wt.\% Li}) - 36.87 \quad \text{(Eq 25b)}$$

These simple expressions permit the calculation of the particle size for the demonstration alloy based on the aging practice and composition parameters.[50]

For Al-Li alloys, the particle size distribution (PSD) can be modeled with the Weibull distribution,[41–51] which has the form given by

$$P(x) = ghX^{h-1} \exp(-gX^h) \quad \text{(Eq 26a)}$$

for $X > 0$, $g > 0$, and $h > 0$

$$P(x) = 0 \text{ elsewhere} \quad \text{(Eq 26b)}$$

and

$$\int_0^\infty P(X)dX = 1 \quad (27)$$

where $P(X)$ is the Weibull probability density function; g and h are the Weibull parameters; and X, which is the normalized particle size diameter, is the ratio of the ith particle diameter d_i to the average particle size diameter $\bar{d}$ for each determined PSD along the precipitation-hardening curve. The value of X is also equivalent to the ratio of the ith particle radius r_i to the average particle size radius $\bar{r}$ of each PSD along the precipitation-hardening curve. For the Al-Li demonstration research alloy, the values for the Weibull parameters can be determined from the empirical relations given by[41–51]

$$g = 0.94 - 0.03 \text{ (wt.\% Li)} \quad \text{(Eq 28a)}$$

$$h = 5.80 - 0.52 \text{ (wt.\% Li)} \quad \text{(Eq 28b)}$$

where g and h are the Weibull distribution parameters given in terms of the weight percent lithium. The equations can also be expressed in terms of the volume fraction of precipitates given by[41–51]

$$g = 0.88 - 0.12\, f_v \quad \text{(Eq 29a)}$$

$$h = 4.69 - 2.17\, f_v \quad \text{(Eq 29b)}$$

where g and h are expressed in terms of the volume fraction of the δ' precipitate phase in the matrix. These Weibull parameters, g and h, are most applicable for the processing of the Al-Li demonstration alloy described in this research. Since these parameters can be affected by processing variables, they may not be universally applicable. Once the PSD and the average particle size have been determined using the analytical models described above, the contributions from the particle shearing and Orowan looping mechanisms to the total strength can be predicted.

5. Results and Discussion

5.1 Predicting the Single Crystal Strength

The single crystal CRSS was determined from the two predominant particle-strengthening mechanisms, *i.e.*, order and Orowan strengthening. The polycrystalline yield strength can be determined directly from the theoretically predicted single crystal strength by determining the appropriate Taylor factor for the given texture and adding any additional contributions that make up the polycrystalline strength. Extruded aluminum alloys develop ⟨111⟩ and ⟨100⟩ fiber textures.[63–67] Additional contributions to the strength may include the intrinsic lattice strength, solid solution strengthening, and strengthening from any Al_3Zr particles distributed in the microstructure. However, any additional strengthening from Al_3Zr is very small.[18,20,21,68] These additional contributions will determine the strength when all of the solute is in solution, *i.e.*, the as-quenched yield strength.

For the Al-Li alloy utilized in this research, a value of 140.6 MPa was determined as an approximation for these contributions. This value was determined by mechanically tensile testing a SHT (0 h aging time) polycrystalline tensile sample of the demonstration Al-Li alloy. Before including these contributions, an approximate value for the Taylor factor of 3[13,69] was utilized for converting the single crystal strength to the polycrystalline shear strength corresponding to the {111}⟨100⟩ duplex fiber texture of the demonstration alloy. Taylor[69] calculated the average orientation factor $\overline{M} = 3.06$[69,70,71] for face-centered cubic polycrystals using a random distribution of grain-orientations. Various investigators[13,15,24,72] have used a Taylor factor of 3 for Al-Li. Broussaud and Diot[66] found $\overline{M}$ to be in the range of 2.45 to 3 for the center of an Al-Li extruded bar. Gomiero *et al.*[25] used a Taylor factor of 2.53 for two different Al-Li alloys compositions.

5.2 Determining the Polycrystalline Strength

In summary, the yield strength can be represented by the expression

$$\sigma_y = \overline{M}\,\Delta\tau_{\text{particle}} + \Delta\sigma_i + \Delta\sigma_{ss} + \Delta\sigma_{gs} \quad \text{(Eq 30)}$$

where $\Delta\tau_{\text{particle}}$ represents the particle-strengthening contribution to the single crystal strength, $\overline{M}$ is the Taylor factor, $\Delta\sigma_i$ represents the intrinsic lattice strength (when no solute is present in solution), and $\Delta\sigma_{ss} + \Delta\sigma_{gs}$ represents the solid solution and grain size strengthening contribution. The intrinsic lattice strength is a result of the inherent lattice resistance to dislocation glide. The total particle-strengthening contribution was due to contributions from both the order and Orowan strengthening mechanisms. The total CRSS based on the particle-strengthening contribution was used in predicting the precipitation-strengthening response of the demonstration alloy.

5.3 Determining the Total Particle-Strengthening Contribution

Various approaches have been taken throughout the literature on summing the contributions from obstacles of various strengths to the CRSS. There has been considerable debate in the literature[12,13,15,18,20,21] as to which approaches are most accurate in determining the additive effects of the contributions to the CRSS. Furukawa *et al.*,[26,27] Tamura *et al.*,[39] and Miura *et al.*[37] claimed that the contributions to the strength are linear. Jensrud[72] assumed that the contributions from the different particle-strengthening mechanisms follow a Pythagorean addition rule. There seems to be no general consensus in the literature for choosing a particular addition rule. However, some of the most common expressions used for adding two particles of different strengths are given by[9,12,20,21]

$$\tau_c = \tau_{c1} + \tau_{c2} \quad \text{(Eq 31a)}$$

$$\tau_c^2 = \tau_{c1}^2 + \tau_{c2}^2 \quad \text{(Eq 31b)}$$

$$\tau_c = \tau_{c1} X_1 + \tau_{c2} X_2 \quad \text{(Eq 31c)}$$

$$\tau_c = \tau_{c1} X_1^5 + \tau_{c2} X_2^{0.5} \quad \text{(Eq 31d)}$$

$$\tau_c^q = \tau_{c1}^q + \tau_{c2}^q \quad \text{(Eq 31e)}$$

where τ_c is the CRSS, q is an adjusted parameter usually ranging from 1 to 2, and X_1 and X_2 are the areal fractions for the particles given be the relationships

$$X_1 = \frac{n_{sl}}{n_s} \quad \text{(Eq 32a)}$$

$$X_2 = \frac{n_{s2}}{n_s} = 1 - X_1 \quad \text{(Eq 32b)}$$

where n_{s1} and n_{s2} are the number particles per unit area for the two different particle mechanisms, *i.e.*, shearable (order) and nonshearable (Orowan) particles; and n_s is the total number of particles per unit area on the given microstructural plane. Equation 31a represents a linear superposition and Eq 31b represents the Pythagorean addition rule. Equations 31c and 32 were utilized in estimating the total particle strengthening based on the contributions of order and Orowan strengthening for the Al-Li demonstration alloy. Thus, the expression for the total particle-strengthening contribution for the demonstration alloy can be expressed as

$$\Delta\tau_{particle} = X_1 \Delta\tau_{order} + X_2 \Delta\tau_{orowan} \quad \text{(Eq 33)}$$

where X_1 and X_2 are defined by Eq 2a and 2b, respectively; and $\Delta\tau_{\text{particle}}$ is the single crystal total particle-strengthening contribution.

The Al-2.6 wt.% Li-0.09 wt.% Zr demonstration alloy was strengthened primarily by the δ' (Al_3Li) precipitates and to a small extent by some Al_3Zr-δ' composite precipitates where the δ' phase coats the Al_3Zr precipitates. Both the δ' and a few composite Al_3Zr-δ' precipitates can be seen in the microstructure of the demonstration alloy illustrated in Fig. 1. Only a relatively small number of the composite Al_3Zr-δ' precipitates exist in the microstructure of the demonstration alloy compared with the large number of δ' particles in the microstructure. This was attributed to the small amount of zirconium (0.09 wt.%) available in the alloy to form the Al_3Zr precipitates. Due the relatively small number of composite Al_3Zr-δ' particles, the effect of these particles on the strength is negligible. Huang[18] and Huang and Ardell[20,21] had found this to be the case for two Al-Li-Cu-Zr alloys, which contained 0.12 wt.% Zr.

The grain size strengthening effect on the yield strength of Al-Li is very small.[13,18,25,72] Thus, the term $\Delta\sigma_{gs}$ in Eq 30 is negligibly small for the Al-Li demonstration alloy. Various investigators have determined the Hall-Petch coefficient for Al-Li alloys to be small, indicating a small grain size strengthening contribution in Al-Li. Jensrud[72] reported a value of only 0.1 MPa$\sqrt{m}$ for the Hall-Petch coefficient of a solution-treated Al-3 wt.% Li alloy. The grain size effect on the yield strength was negligible.[72] For a peak-aged Al-2 wt.% Li-2 wt.% Mg alloy, Dinsdale *et al.*[73] reported a value of 0.23 MPa$\sqrt{m}$ for the Hall-Petch coefficient. In aluminum alloys, the Hall-Petch parameter varies from 0.06 MPa to 0.25 MPa$\sqrt{m}$[72] depending on the aging condition.

A computer model was developed to perform the calculations for the CRSS for each particle-strengthening mechanism, the total CRSS, the total particle-strengthening response, the polycrystalline strength, and the overall precipitation strengthening response. The computer program includes all of the previously discussed analytical expressions, including the expressions for the Weibull distribution function, necessary for predicting the strength. The input to the program includes the aging times, the aging temperature, the Orowan looping radius, the composition, the Taylor factor, the solid solution and grain size strengthening contribution, and the values of the constants used for the CRSS strengthening mechanisms. The constants used as input include the Burgers vector, the shear moduli of the matrix and precipitate phases, the antiphase boundary energy, the volume fraction, and the Poisson's ratio. Also, because of the constancy of the volume fraction of δ', the matrix CRSS has to be taken as constant.[18] The distribution of particle sizes for each aging time was used as input to the strength model rather than an average particle size since the size distribution was more representative of real microstructures. Figure 1(a) and (b) show the microstructure with the δ' PSD of the Al-Li-Zr research alloy for the underaged and overaged conditions, respectively. The PSD was determined from the microstructural model[41–51] used to predict the microstructure of Al-Li alloys. A PSD of approximately 200 particles of different sizes predicted from the microstructural model for each given aging time was used to predict the strength at each given aging time. In order to perform the calculations, the computer program calculates the stress necessary to either shear or loop each particle depending on particle size and spacing. Particles that were larger than the looping radius were analyzed by the Orowan looping model, and particles smaller than the looping radius were analyzed by the order hardening model. The total stress necessary for both dislocation shearing and dislocation looping was determined for each given aging time

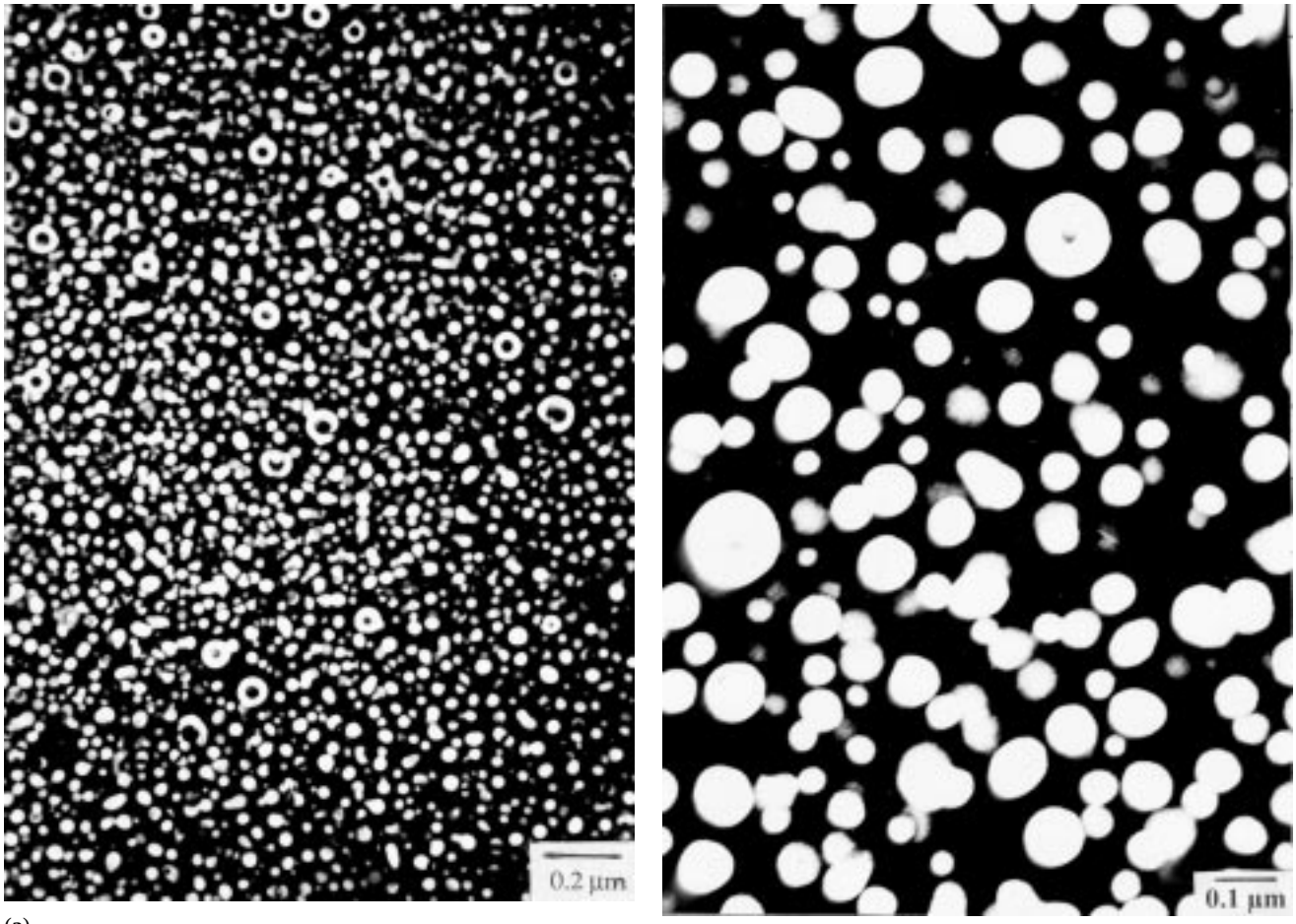

(**a**) (**b**)

Fig. 1 (**a**) Transmission electron micrograph dark-field image showing the microstructure of the Al-2.6 wt.% Li-0.09 wt.% Zr demonstration alloy in the underaged condition, aged at 185 °C for 24 h, obtained from photographed thin foil specimens. (**b**) Transmission electron micrograph dark-field image showing the microstructure of the Al-2.6 wt.% Li-0.09 wt.% Zr demonstration alloy in the overaged condition, aged at 185 °C for 96 h, obtained from photographed thin foil specimens.

along the age-hardening curve. Once the total stress for dislocation shearing and dislocation looping has been determined, the computer calculates the CRSS for the strengthening mechanisms. The total CRSS is determined for each aging time along the age-hardening curve and the polycrystalline yield strength is determined for each aging time along the age-hardening curve. Hence, the precipitation-strengthening response is predicted from the computer model from the given input components, *i.e.*, the heat treatment, composition, and aging practice (temperature and time). The results in Tables 4 and 5, which summarize the predicted results for order and Orowan strengthening, the total particle-strengthening contribution, and the predicted yield strength values for the 185 °C and 193 °C aging treatments, were determined utilizing the PSDs from the Weibull probability density function. The 193 °C aging practice had a much faster aging response than did the 185 °C aging practice. The faster aging response of the 193 °C temper compared with the 185 °C temper could be seen in the peak-aging times of the different aging treatments. The peak-aging time for the 185 °C aging practice was approximately 48 h, whereas the peak-aging time for the 193 °C aging practice was only around 18 h. Wang and Wells[68] found that an aging temperature of 195 °C or greater is too high for Al Li because overaging occurs in less than 1 h due to rapid coarsening of the δ' phase, which results from the high diffusion rate of lithium.[68] It is known that in Al-Li alloys, both the nucleation and growth of δ' are extremely rapid.[53,62,74] The experimentally measured yield strength values are also given in Tables 4 and 5 as a direct comparison with the predicted values. In addition, the predicted precipitation strengthening responses for the 185 °C and 193 °C aging practices of the demonstration alloy, which are shown in Fig. 2 and 3, respectively, were determined from Eq 30 and are based on the total particle-strengthening contribution. The predicted aging curves were in good agreement with the experimental results for both aging tempers. However, in the underaged condition at aging times less than 2 h, the model overpredicted the aging response. This may possibly be due to slightly high values used for some of the microstructural constants such as the equilibrium volume fraction or antiphase boundary energy. However, it is very difficult to determine

Table 4. Comparison between the experimentally measured yield strength and the theoretically predicted precipitation strengthening response for the Al-2.6 wt.% Li 0.09 wt.% Zr research alloy aged at 185 °C

Aging time t (h)	Order strengthening $\Delta\tau_{order}$ (MPa)	Orowan strengthening $\Delta\tau_{orowan}$ (MPa)	Particle strengthening $\Delta\tau_{particle}$ (MPa)	Predicted strength (MPa)	Yield strength σ_y (MPa)
0.12	63.9	0.0	63.9	332.2	⋯
0.25	68.1	0.0	68.1	344.8	295.0
0.50	72.7	0.0	72.7	358.7	312.3
1.0	78.0	0.0	78.0	374.6	339.1
2.0	84.0	0.0	84.0	392.3	372.9
4.0	90.8	0.0	90.8	412.9	398.4
8.0	96.7	73.5	96.3	429.5	448.0
12.0	100.7	77.1	100.1	441.0	⋯
18.0	103.9	85.0	102.6	448.3	437.0
24.0	105.6	86.6	103.0	449.7	⋯
32.0	106.5	86.4	101.7	445.7	⋯
40.0	105.9	86.3	98.5	436.0	⋯
48.0	104.0	86.3	94.4	423.9	449.4
72.0	104.3	80.9	88.1	404.8	436.3
96.0	102.6	77.4	81.8	386.1	415.0
120.0	105.5	73.2	78.9	377.3	⋯
180.0	105.0	67.4	70.5	352.0	⋯
225.0	99.8	64.6	65.1	335.9	328.8

Table 5. Comparison between the experimentally measured yield strength and the theoretically predicted precipitation strengthening response for the Al-2.6 wt.% Li-0.09 wt.% Zr research alloy aged at 193 °C

Aging time t (h)	Order strengthening $\Delta\tau_{order}$ (MPa)	Orowan Strengthening $\Delta\tau_{orowan}$ (MPa)	Particle Strengthening $\Delta\tau_{particle}$ (MPa)	Predicted Strength (MPa)	Yield Strength σ_y (MPa)
0.12	66.1	0.0	66.1	338.9	⋯
0.25	70.7	0.0	70.7	352.8	298.5
0.50	75.8	0.0	75.8	367.9	324.7
1.0	81.5	0.0	81.5	385.0	352.3
2.0	87.9	0.0	87.9	404.3	383.3
4.0	94.5	50.0	94.3	423.4	422.6
8.0	100.8	77.1	100.2	441.1	430.8
12.0	103.9	84.9	102.6	448.4	426.0
18.0	104.4	90.0	100.9	443.4	432.9
24.0	104.6	88.5	98.5	436.0	428.8
32.0	104.0	86.2	94.4	423.8	⋯
40.0	105.9	81.6	93.3	420.4	⋯
48.0	104.4	80.8	88.0	404.7	410.2
72.0	104.2	75.1	80.2	381.2	401.9
96.0	102.0	71.3	73.7	361.8	374.3
120.0	105.0	67.4	70.4	351.8	⋯
180.0	102.3	61.6	62.2	327.3	⋯
225.0	105.3	58.2	58.9	317.3	321.9

exact values for these microstructural parameters. To better understand the effects of the microstructural parameters, a sensitivity study on the different microstructural constants was used to determine their individual effects on the precipitation-strengthening curve. From this study, it was found that the antiphase boundary energy had the largest effect from particle shearing of the different constants on the precipitation-strengthening response in the demonstration alloy.

6. Summary and Conclusions

- An Al-Li alloy system was used as a vehicle for the development of a model that predicts the precipitation-strengthening response, *i.e.*, the variation in yield strength with aging time, from the composition and the heat treatment processing variables.

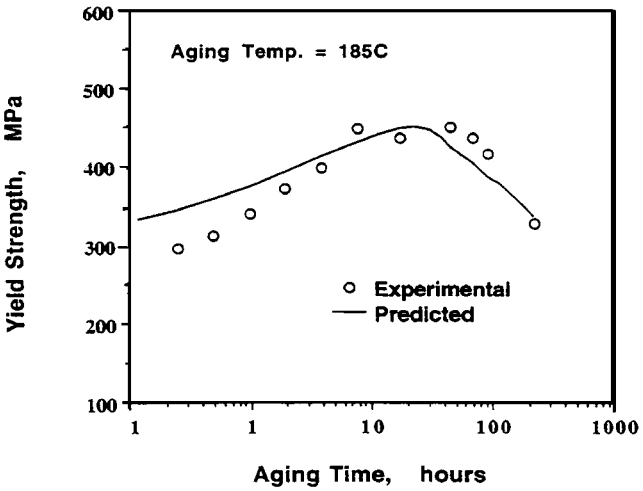

Fig. 2 Comparison between the experimentally measured and the theoretically predicted precipitation strengthening response for the Al-2.6 wt.% Li-0.09 wt.% Zr demonstration alloy aged at 185 °C.

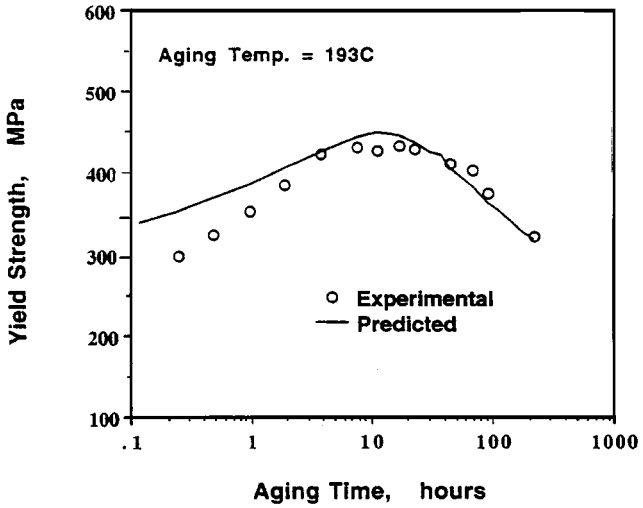

Fig. 3 Comparison between the experimentally measured and the theoretically predicted precipitation strengthening response for the Al-2.6 wt.% Li-0.09 wt.% Zr demonstration alloy aged at 193 °C.

- Order hardening and Orowan strengthening were the primary mechanisms responsible for controlling the aging response for the Al-Li demonstration alloy. The precipitation-hardening response, which was approximated from the heat treatment, composition, and microstructure, was based on the order and Orowan particle-strengthening mechanisms. Order hardening was found to dominate the strengthening in the underaged and peak-aged conditions, and Orowan strengthening dominated the strengthening in the overaged condition.
- The yield strength was predicted using the PSD, *i.e.*, the distribution of particle sizes predicted from the microstructural model, at each aging time along the precipitation-hardening response rather than an average particle size. A constant value for the equilibrium volume fraction was utilized in predicting the precipitation-strengthening response. The predicted age-hardening curves were in good agreement with the experimental results. However, in the underaged condition under 2 h aging time, the model overpredicted the yield strength.

Acknowledgments

This work was supported by the National Science Foundation under Grant No. CDR 8803017. The Al-Li alloy used for this study was provided by ALCOA and was cast at their Technical Center (Pittsburgh, PA). The Al-Li alloy was extrusion processed by the ALCOA Lafayette Extrusion and Tube Division (Lafayette, IN). The composition analysis for the Al-Li alloy was also performed by the ALCOA Extrusion Facility.

References

1. H. Gleiter and E. Hornbogen: *Mater. Sci. Eng.*, 1968, vol. 2, pp. 285-302.
2. V. Gerold and H. Haberkorn: *Phys. Status Solidi*, 1966, vol. 16, pp. 675-84.
3. P.B. Hirsch and A. Kelly: *Phil. Mag.*, 1965, vol. 12, pp. 881-900.
4. K.C. Russell and L.M. Brown: *Acta Metall.*, 1972, vol. 20, pp. 969-74.
5. A. Melander and P.A. Persson: *Acta Metall.*, 1978, vol. 26, pp. 267-78.
6. E. Nemback: *Acta Metall.*, 1983, vol. 26, pp. 267-68.
7. G. Knowles and P.M. Kelly: *Effect of Second-Phase Particles on the Mechanical Properties of Steel* The Iron and Steel Institute, London, 1971, p. 9.
8. A. Kelly and M.E. Fine: *Acta Metall.*, 1957, vol. 5, pp. 365-67.
9. L.M. Brown and R.K. Ham: *Strengthening Methods in Crystals*, John Wiley & Sons, New York, NY, 1971.
10. H. Gleiter and E. Hornbogen: *Phys. Status Solidi*, 1965, vol. 12, pp. 251-64.
11. H. Gleiter: *Acta Metall.*, 1968, vol. 16, pp. 829-30.
12. A.J. Ardell: *Metall. Trans. A*, 1985, vol. 16, pp. 2131-65.
13. J. Glazer: Master's Thesis, University of California, Los Angeles, CA, 1986.
14. E. Orowan: "Symposium on Internal Stresses in Metals and Alloys," *Sess. III Disc. Inst. Met.*, 1948, p. 451.
15. J. Glazer and J.W. Morris: *Acta Metall.*, 1988, vol. 36 (4), pp. 907-15.
16. *Annual Book of ASTM Standards*, ASTM, Philadelphia, PA, 1988, vol. 3.01, sect. 3.
17. P.C. McKeighan: "Summary of Tensile Testing Al-2.6 wt.% Li-0.09 wt.% Zr Alloy," Purdue NSF-Sponsored ERC Project Program Inception Report, Purdue University, West Lafayette, IN, 1991.
18. J.C. Huang: Ph.D. Dissertation, University of California, Los Angeles, CA, 1986.
19. J.C. Huang and A.J. Ardell: *Alum. Technol.*, 1986, vol. 86, pp. 434-41.
20. J.C. Huang and A.J. Ardell: *Mater. Sci. Eng.*, 1988, vol. A104, pp. 149-56.
21. J.C. Huang and A.J. Ardell: *Acta Metall.*, 1988, vol. 36 (11), pp. 2995-3006.
22. P. Sainfort and P. Guyot: *Aluminum-Lithium Alloys III*, The Institute of Metals, London, 1986, pp. 420-26.
23. J. Glazer, T.S. Edgecumbe, and J.W. Morris, Jr.: *Aluminum-Lithium Alloys III*, The Institute of Metals, London, 1986, pp. 369-75.
24. B. Noble, S.J. Harris, and K. Dinsdale: *Met. Sci.*, 1982, vol. 16, pp. 425-30.
25. P. Gomiero, Y. Brechet, F. Louchet, A. Tourabi, and B. Wack: *Acta Metall. Mater.*, 1992, vol. 40 (4), pp. 857-61.
26. M. Furukawa, Y. Miura, and M. Nemoto: *Trans. Jpn. Inst. Met.*, 1985, vol. 26 (4), pp. 225-29.

27. M. Furukawa, Y. Miura, and M. Nemoto: *Trans. Jpn. Inst. Met.*, 1985, vol. 26 (4), pp. 230-35.
28. J.W. Martin: *Micromechanisms in Particle-Hardened Alloys*, Cambridge University Press, Oxford, United Kingdom, 1980, pp. 50-79.
29. A.J.E. Foreman and M.J. Makin: *Can. J. Phys.*, 1957, vol. 45, pp. 511-17.
30. U.F. Kocks: *Phil. Mag.*, 1966, vol. 13, p. 541.
31. M.F. Ashby: *Acta Metall.*, 1966, vol. 14, p. 679.
32. P. Sainfort and P. Guyot: *Proc. 7th Int. Conf. on the Strength of Metals and Alloys*, 1985, vol. 1, p. 441.
33. M. Tamura, T. Mori, and T. Nakamura: *J. Jpn. Inst. Met.*, 1970, vol. 34, pp. 919-25.
34. A.J. Ardell and J.C. Huang: *Phil. Mag. Lett.*, 1988, vol. 58 (4), pp. 189-97.
35. G. De Wit and J.S. Koehler: *Phys. Rev.*, 1959, vol. 116 (5), pp. 1113-20.
36. P.B. Hirsch and F.J. Humphreys: *Physics of Strength Plasticity*, Massachusetts Institute of Technology Press, Cambridge, MA, 1969, p. 189.
37. Y. Miura, A. Matsui, M. Furukawa, and M. Nemoto: *Aluminum-Lithium Alloys III*, TMS-AIME, Warrendale, PA, 1986, pp. 427-34.
38. W. Muller, E. Bubeck, and V. Gerold: *Aluminum-Lithium Alloys III*, TMS-AIME, Warrendale, PA, 1986, pp. 435-41.
39. M. Tamura, T. Mori, and T. Nakamura: *Trans. Jpn. Inst. Met.*, 1973, vol. 114, pp. 355-63.
40. K. Mahalingam: Purdue University, West Lafayette, IN, personal communication, Apr. 17, 1992.
41. B.P. Gu, S.C. Jha, G.L. Liedl, K. Mahalingam, and T.H. Sanders, Jr.: *Light Met.*, 1985, pp. 35-43.
42. B.P. Gu, G.L. Liedl, T.H. Sanders, Jr., and K. Welpmann: *Mater. Sci. Eng.*, 1985, vol. 76, pp. 147-57.
43. B.P. Gu, K. Mahalingam, G.L. Liedl, and T.H. Sanders, Jr.: *Aluminum-Lithium Alloys III*, The Institute of Metals, London, 1986, pp. 360-68.
44. B.P. Gu, G.L. Liedl, K. Mahalingam, and T.H. Sanders, Jr.: *Mater. Sci. Eng.*, 1986, vol. 78, pp. 71-85.
45. B.P. Gu, G.L. Liedl, K. Mahalingam, and T.H. Sanders, Jr.: *Unusual Tech. New Appl. Metallogr.*, 1986, vol. 24.
46. B.P. Gu: Ph.D. Dissertation, Purdue University, West Lafayette, IN, 1985.
47. S.C. Jha, K. Mahalingam, and T.H. Sanders, Jr.: *Alum. Alloys: Their Physical Mech. Prop.*, 1986, vol. 2, pp. 677-93.
48. S.C. Jha, T.H. Sanders, Jr., and M.A. Dayananda: *Acta Metall.*, 1987, vol. 35 (2), pp. 473-82.
49. S.C. Jha: Ph.D. Dissertation, Purdue University, West Lafayette, IN, 1987.
50. K. Mahalingam, B.P. Gu, G.L. Liedl, and T.H. Sanders, Jr.: *Acta Metall.*, 1987, vol. 35 (2), pp. 483-98.
51. K. Mahalingam: Ph.D. Dissertation, Purdue University, West Lafayette, IN, 1989.
52. P. Sainfort and P. Guyot: *Strength of Metals and Alloys*, Pergamon Press, Oxford, United Kingdom, 1985, p. 441.
53. J.H. Kulwicki, and T.H. Sanders, Jr.: *Aluminum-Lithium Alloys II*, TMS-AIME, Warrendale, PA, 1986, pp. 31-51.
54. S.F. Baumann and D.B. Williams: *Scripta Metall.*, 1984, vol. 18, pp. 611-16.
55. I.M. Lifshitz and V.V. Slyozov: *J. Phys. Chem. Solids*, 1961, vol. 19, pp. 35-50.
56. C. Wagner: *Z. Elekrochemie*, 1961, vol. 3 (7), pp. 581-91 (in German).
57. A.J. Ardell: *Acta Metall.*, 1972, vol. 20, pp. 61-71.
58. A.D. Brailsford and P. Wynblatt: *Acta Metall.*, 1979, vol. 27, pp. 489-97.
59. C.K.L. Davies, P. Nash, and R.N. Stevens: *Acta Metall.*, 1980, vol. 28, pp. 179-89.
60. H.R. Shercliff and M.F. Ashby: Report No. CUED/C-Mat./TR156, Cambridge University, Cambridge, United Kingdom, 1989.
61. O. Jensrud and N. Ryum: *Mater. Sci. .Eng.*, 1984, vol. 64, pp. 229-36.
62. D.B. Williams and J.W. Edington: *Met. Sci. J.*, 1975, vol. 9, pp. 529-32.
63. A.W. Bowen: *Mater. Sci. Technol.*, 1990, vol. 6, pp. 1058-71.
64. I. Dillamore and W. Roberts: *Metall. Rev.*, 1965, vol. 10 (39), pp. 271-372.
65. H. Hu: *Texture*, 1974, vol. 1, pp. 233-58.
66. F. Broussaud and C. Diot: *J. Phys.*, 1987, vol. 48 (9), pp. 597-603.
67. G. Tempus, G. Scharf, and W. Calles: *J. Phys.*, 1987, vol. 48 (9), pp. 187-93.
68. W. Wang and G.H. Wells: *Light Weight Alloys for Aerospace Applications II*, 1991, vol. 2, pp. 189-202.
69. G.J. Taylor: *J. Met.*, 1938, vol. 62, pp. 307-25.
70. S. Howe and C. Elbaum: *Phil. Mag.*, 1961, vol. 6, pp. 37-48.
71. A.W. Thompson: *Metall. Trans.*, 1974, vol. 5, pp. 39-42.
72. O. Jensrud: *Aluminum-Lithium Alloys III*, The Institute of Metals, London, 1985, pp. 411-19.
73. K. Dinsdale, S.J. Harris, and B. Noble: *Aluminum-Lithium Alloys*, TMS-AIME, Philadelphia, PA, 1981, p. 101.
74. B. Noble and G.E. Thompson: *Met. Sci. J.*, 1971, vol. 5, pp. 114-20.